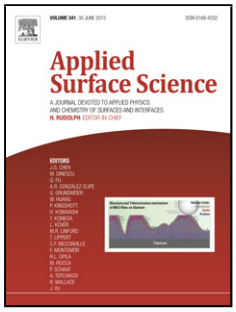

Title: Reduced graphene oxide wrapped hierarchical TiO_2 nanorod composites for improved charge collection efficiency and carrier lifetime in dye sensitized solar cells

Authors: Mohan Raj Subramaniam, Duraisamy Kumaresan, Sathiskumar Jothi, James D. McGettrick, Trystan M. Watson

PII: S0169-4332(17)32790-3
DOI: http://dx.doi.org/10.1016/j.apsusc.2017.09.142
Reference: APSUSC 37221

To appear in: *APSUSC*

Received date: 11-5-2017
Revised date: 21-8-2017
Accepted date: 17-9-2017

Please cite this article as: Mohan Raj Subramaniam, Duraisamy Kumaresan, Sathiskumar Jothi, James D.McGettrick, Trystan M.Watson, Reduced graphene oxide wrapped hierarchical TiO2 nanorod composites for improved charge collection efficiency and carrier lifetime in dye sensitized solar cells, Applied Surface Sciencehttp://dx.doi.org/10.1016/j.apsusc.2017.09.142

Reduced graphene oxide wrapped hierarchical TiO_2 nanorod composites for improved charge collection efficiency and carrier lifetime in dye sensitized solar cells

Mohan Raj Subramaniam,[a b] *Duraisamy Kumaresan,**[a b] *Sathiskumar Jothi,*[c] *James D McGettrick*[c] *and Trystan M Watson*[c d]

a. Department of Chemical Engineering and Materials Science, Amrita School of Engineering, Coimbatore 641112, Amrita Vishwa Vidyapeetham University, Amrita University, INDIA. E-mail: rdkumares@gmail.com; Fax: +91-422-2656274; Tel: +91-422-2685000.

b. Center of Excellence in Advanced Materials and Green Technologies, Amrita School of Engineering, Coimbatore 641112, Amrita Vishwa Vidyapeetham, Amrita University, INDIA.

c. College of Engineering, Swansea University, Bay campus, Swansea, SA1 8EN, UK.

d. SPECIFIC, Swansea University, College of Engineering, Engineering East, Bay Campus, Swansea, SA1 8EN, UK.

Graphical Abstract

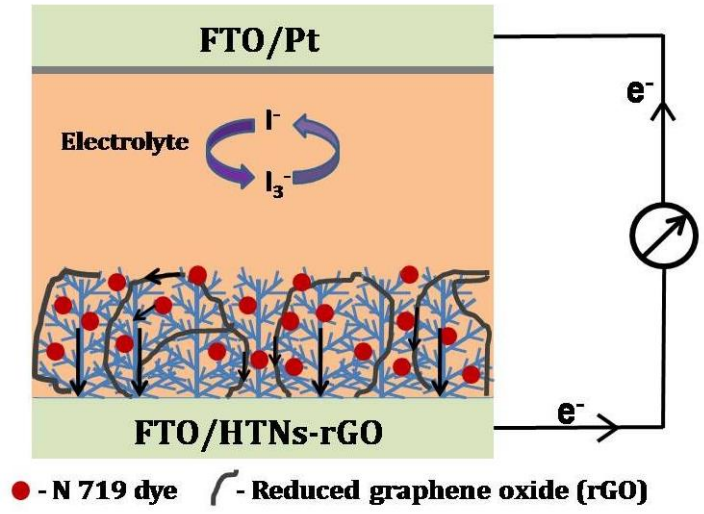

Reduced graphene oxide incorporated hierarchical TiO_2 nanorods based nanocomposites for improving the charge collection efficiency and photovoltaic performance in dye sensitized solar cells are introduced.

Highlights

- Reduced graphene oxide-hierarchical TiO_2 nanorod composites were prepared
- The nanocomposites were tested as photoanodes of dye sensitized solar cells (DSSCs)
- Wt% of reduced graphene oxide in composites affected the charge transfer at interface
- 2 wt% of reduced graphene oxide improved PCE about 47% in TiO_2 nanorod based DSSCs.

Abstract

Three dimensional hierarchical TiO_2 nanorods-reduced graphene oxide (HTNs-rGO) composites with different rGO wt% were directly grown on conducting glass substrate by an in situ hydrothermal process for improved charge separation and collection in dye sensitized solar cells (DSSCs). The crystal structure and chemical composition of as grown composites were confirmed by X-ray diffraction and optical studies. Electron microscopic studies on the composites surface morphologies revealed the formation of rGO wrapped or intertwined HTNs architectures onto the FTO substrates with thicknesses ranging from 14.33 to 15.70 μm. 2 wt% rGO loaded HTNs composite photoanode showed a superior power conversion efficiency of 4.54% as compared to the other wt% rGO loaded HTNs composite and bare HTNs photoanodes in DSSCs. This is due to optimal loading of rGO facilitating formation of a better charge transport channel within HTNs matrix and reducing charge transport resistance (R_{tr}), which resulted in a higher charge collection of HTNs-rGO composite. Besides, the solar cell current-voltage (J-V) and electrochemical impedance characterizations confirmed the superior light scattering and dye loading capabilities of HTNs, together with a low charge transport resistance and improved charge carrier lifetime in HTNs-rGO composites contributed to the photovoltaic performance enhancement of their DSSCs.

Keywords: *Hierarchical TiO_2 nanorods, reduced graphene oxide, hydrothermal, charge collection efficiency, dye-sensitized solar cells.*

1. Introduction

The dye-sensitized solar cells (DSSCs) are widely accepted as one of the most promising solar energy conversion devices by the photovoltaic community, because of their relatively low cost, environmentally benign fabrication process and high power conversion efficiency (PCE) [1, 2]. In the past two decades, many efforts have been devoted to increase the efficiency by different research groups in worldwide and as a result the PCE of DSSC improved up to 13 % [3, 4]. Usually a DSSC is constructed in sandwich-type device configuration constituted by a photoanode, an electrolyte and a photocathode. Among these major components, the semiconducting nanomaterial used for the fabrication of DSSC photoanode has received a large attention because of its indispensable role in the photo-induced electron generation and transport to the collector electrode connected to the external load, which influences heavily the photo-current density and power conversion efficiency of DSSC. In photoanode, usually dye connected TiO_2 nanoparticles has been preferably used as semiconducting nanomaterial for visible light absorption of DSSC because of its high internal surface area aiding a superior dye loading and its low-cost optimized synthesis process by a chemical route [5]. But, TiO_2 nanoparticles produce more grain boundaries in the interconnected nanoparticles network that can hinder the electron transport, and increase the interfacial charge recombination between photogenerated electron and positive species of the electrolyte [6].

To overcome this, one dimensional (1D) nanostructures such as nanowires, nanorods and nanotubes have been employed to provide direct charge transport channels from the place of charge injection to the conducting film of collector electrode [7, 8]. Also, more perceptibly single crystal nanowires have shown up to 100 times higher electron transport than the nanoparticles [9]. A fast electron transport of these 1D nanostructures reduces the interfacial charge recombination between photogenerated electron and electrolyte positive species. However, these 1D nanostructures have smaller surface areas as compared to the nanoparticles, so they cannot not anchor enough dye molecules on surfaces of their porous networks to produce more photogenerated electrons. To address this issue, well aligned nanowires and nanorods composed of small oxide particles have been used as photoanode materials. This has improved surface area, light scattering ability and porous structures significantly, which facilitate better electrolyte diffusion to achieve superior performing DSSCs [10]. Alternatively, multi-dimensional hierarchical TiO_2 nanostructures have been considered as superior light scattering materials for

improving the light harvesting and power conversion efficiencies of DSSCs and graphene-TiO_2 nanoparticles composites have also been demonstrated to solve all these problems to a considerable extent [11, 12]. Moreover, introducing thin, high electron conducting materials for instance graphene in to TiO_2 matrix has improved the electron diffusion length and lifetime in the graphene-TiO_2 composite photoanodes which reduces the recombination losses.

Graphene is a one atomic thick, ideal two dimensional (2D) sheet formed by sp^2 bonded carbon atoms network has received a lot of attention since after its discovery in 2004 because of its distinctive physicochemical properties [13]. It is a zero band gap material exhibits excellent mobility of charge carriers (200000 $cm^2V^{-1}s^{-1}$), a very high theoretical surface area (2600 m^2g^{-1}) and low visible light absorption property [14, 15]. Because of these anomalous properties, graphene is very much attractive in several device fabrications including DSSCs [16, 17]. Usually a chemically exfoliated graphite oxide (GO) conversion to single layered reduced graphene oxide (rGO) is considered good replacement material for the graphene due to the synthetic difficulties of obtaining a pure graphene monolayer. Further, from chemical point of view the presence of oxygen functionalities at a GO or rGO surface is very interesting because it provides more reactive sites for the preparation of new graphene based derivatives and composite materials [18]. Moreover, incorporation of rGO in TiO_2 nanoparticles network has been considered interesting for improving surface area, chemical stability, and electrical conductivity in the DSSC applications. Therefore, many literature reports have been published using TiO_2-rGO composites as electrode materials of DSSCs [19-21]. The incorporation of rGO improves the photovoltaic performance of TiO_2 nanoparticles based DSSCs by increasing electron transport within the TiO_2 nanoparticles network and by reducing the charge recombination processes. Thus, the TiO_2 nanoparticles based TiO_2-rGO nanocomposite photoanodes in dye-sensitized solar cells have produced power conversion efficiency up to 8.62 % are known [22, 23]. Alternatively, self-assembling TiO_2 nanorods on large graphene oxide sheets at a two-phase interface for the improved anti-recombination properties in photocatalytic applications has been reported recently by Jincheng Liu and coworkers [24].

Furthermore, the TiO_2 nanorods/nanowires and its hierarchical architectures are considered as effective DSSC photoanode materials because of their superior light harvesting, charge transport properties and capable of functioning as superior light-scattering layers [6, 9]. However, the fabrication of TiO_2 nanorod-rGO composites based DSSC photoanodes and their photovoltaic

performance are not familiar with the literature. Therefore, in this paper, we have reported a facile in situ method for the growth of rGO incorporated hierarchical TiO_2 nanorod (HTNs-rGO) composites on FTO substrates for improving the TiO_2 nanorod based DSSCs photovoltaic performance. Moreover, we have analyzed and reported the interfacial charge transfer processes at the photoanode/electrolyte interfaces of HTNs-rGO composites in DSSCs using electrochemical impedance spectroscopy to demonstrate the influence of rGO wt% in the charge collection and transfer of their respective photoanodes.

2. Materials and Methods

Different HTNs-rGO composites were directly grown on FTO substrate by an in situ hydrothermal method using mixtures of Ti precursor and rGO dispersion, wherein GO and rGO were used as-prepared by following the procedures modified from literature reports given in the supporting information. The rGO with different weight ratio (0.0, 0.4, 1.2 and 2.0%) was dispersed in 1:1 volume ratio (15 mL: 15 mL) of acid and 100 µM aqueous solution of sodium dodecyl sulfate (SDS) mixture. And, 1 mL of titanium isopropoxide (TTIP) was added drop wise to this mixture and then it was transferred to Teflon lined autoclave and heat treated for digestion at 210 °C temperature for 2 hours wherein the FTO substrate was placed horizontally with conducting side facing up (Scheme 1). After the hydrothermal process, each HTNs-rGO composite grown FTO substrate was rinsed thoroughly using DI water and ethanol. The HTNs films incorporated with rGO are indicated as HTNs-0.0% rGO, HTNs-0.4% rGO, HTNs-1.2% rGO, and HTNs-2.0% rGO corresponding to the rGO weight ratio. The as-prepared HTNs-rGO composites were used as photoanodes, after coating with N719 dye, for the DSSC fabrication by following the procedure reported in literature [11].

The absorbance spectra of thin films were obtained using Shimadzu 2600 UV-visible absorbance spectrophotometer in the spectral range 200-800 nm. Raman spectra were recorded in a BRUKER RFS 27: stand alone FT-Raman Spectrometer (laser source is Nd: YAG 1064 nm) from the spectral range 50 cm^{-1} to 4000 cm^{-1}. Fourier transform infrared spectra (FTIR) were recorded in a Thermo Nicolet, iS10 FTIR spectrometer using ATR mode in the range 400-4000 cm^{-1}. The X-ray powder diffraction patterns (XRD) were recorded using a PANalytical's X'Pert PRO X-ray diffractometer (Cu-Kα radiation) at 0.02/sec as the step interval. X-ray photoelectron spectroscopy (XPS) analysis was done using ultra high vacuum (1×10^{-10} mbar) instrument attached with the monochromatic Al Kα (1.486 KeV) X-ray resource, hemi-spherical electron

energy analyzer (SPECS Phoibos 150), and delay-line detector. The FESEM images of samples were obtained in a FEI Quanta 200 high resolution scanning electron microscope. High resolution transmission electron microscopy (HRTEM) analysis was carried out using a JEOL JEM 2100 TEM. The powdered samples were dispersed in ethanol solution and drop casted on the carbon coated copper grid (200 mesh), dried and analyzed. The DSSCs current-voltage (I-V) performances were recorded under one sun illumination using AM 1.5G filter equipped Newport xenon source and 2400 Keithley solar cell characterization setup. The EIS analysis was done using CHI604E electrochemical analyzer, USA. The incident photon-to-current conversion efficiency (IPCE) was recorded using a Newport-Oriel setup consisting of a cornerstone monochromator, a 300W ozone free xenon lamp and a calibrated photodiode.

3. Results and discussion

The electronic interactions of HTNs and rGO in HTNs-rGO composites are studied by UV-visible diffused reflectance spectroscopy. As shown in Fig. 1a, the bare HTNs has showed a strong absorption in the UV region (< 400 nm), resulting from the electronic transitions between the valence and conduction band of TiO_2. However, more broad absorptions observed in the visible region for different HTNs-rGO composites with higher wt% of rGO, are attributed to the visible light absorption characteristic of rGO in HTNs-rGO composites. Usually GO and rGO aqueous dispersions demonstrate strong absorption bands in the UV-region (supporting information Fig. S1). In the GO absorption spectrum, a peak observed around 232 nm and a shoulder at 296 nm with the absorption tailing up to 800 nm is attributed mainly to the π-π^* transition of C=C and n-π^* transition of C=O functionalities, respectively [25]. In case of rGO, the absorption peak at 232 nm is disappeared or red shifted to 271 nm may be due to the extension of conjugation, which suggests the reduction of GO to rGO. Due to the strong electronic interactions between the rGO and HTNs, the HTNs-2.0% rGO composite displays a noticeable red shift of absorption edge, which hints the band gap narrowing in HTNs-rGO composites [26]. Furthermore, the band gap energies of the HTNs and HTNs-rGO composites are determined according to the plot in Fig. 1a (inset). As shown in the plot, the band gap energies of bare HTNs, 0.4%, 1.2% and 2.0% rGO containing HTNs-rGO composite films are 3.07, 3.06, 3.06 and 3.04 respectively, indicating the increase of rGO content influencing the TiO_2 conduction band edge of the composites. Further, these results indicate that there could be some amount of Ti-O-C bonds formation between HTNs and rGO sheets in composites.

FTIR analysis was carried on to observe the extent of reduction of GO to rGO and to analyze the interactions between HTNs and rGO in the HTNs-rGO composites. As shown in Fig. 1b, the GO exhibited several characteristic IR absorption peaks for oxygen containing groups. The absorption peaks were appeared in the frequency regions 862 cm^{-1} accounted for the aromatic C-H deformation, 1,046 cm^{-1} for C-O stretching, 1,215 cm^{-1} for phenolic C-OH stretching, 1732 cm^{-1} for the stretching mode of carboxylic moieties (C=O group) and a broad peak around 3,400 cm^{-1} for the O-H stretching vibrations of C-OH groups. Also Fig. 1b shows the intensity of IR peaks reduced drastically at 1732 cm^{-1} and 1215 cm^{-1} in rGO and HTNs-rGO composite, simultaneously a pronounced peak appeared at 1573 cm^{-1} for C=C bonds corroborated the effective reduction of GO to rGO. The reduced peak intensity of GO at 3400 cm^{-1} (O-H stretch) could be due to the reduction of GO to rGO. Further, a weak and broad band observed at 600-900 cm^{-1} for HTNs-2.0% rGO composite indicate the Ti-O-Ti stretching vibration mode, a characteristic of the HTNs. And the peak observed at 1443 cm^{-1} could be due to the carbon skeleton vibration (of C-O) in HTNs-2.0% rGO composite due to the bonding interactions of HTNs and rGO [27, 28].

Fig. 2 shows the powder XRD patterns of GO, rGO, HTNs and HTNs-2.0% rGO composite. The XRD pattern of GO showed a characteristic peak at 10.50° (001) which confirmed that most of the graphite powder was oxidized into GO by expanding their interlayer d spacing from 0.34 nm to 0.94 nm [29]. The increased interlayer distance of GO can be assigned to the existence of more oxygen-containing functionalities such as hydroxyl, carbonyl and carboxyl groups. And the XRD pattern of rGO and HTNs-rGO composite exhibited a broad peak around 26°. Further the disappearance of GO peak, suggesting that the GO was transformed to rGO almost completely in the reduction process [30]. Also, the vanishing GO XRD peak indicated that the GO layers were transformed into rGO sheets. However, the representative peak of graphene sheets (2θ = 25.4°) was not appeared either. Furthermore, the XRD patterns of HTNs and HTNs-2.0% rGO composite films confirmed the presence of pure rutile phase TiO_2 by showing sharp diffraction peaks for (110), (101), (111), (211), (002) and (301) (JCPDS card No. 21-1276) planes of the highly crystalline HTNs and HTNs-rGO composite. The diffraction peaks for additional phases or impurities were not seen in XRD patterns which further confirmed the purity and high crystallinity of HTNs of the composites. In addition, the characteristic diffraction peak of rGO was not easily detected in the XRD pattern of the HTNs-2.0% rGO composite. However, a weak

peak around 26° angle was appeared in the HTNs-rGO composite XRD due to the rGO peak superimposed with more intense TiO_2 (101) peak and the low concentration presence of rGO in the composite materials [31].

Raman spectroscopy was used for the analysis of defects and structures of HTNs-rGO composites. The Raman intensity ratio of the D (appears at 1355 cm^{-1}) and G (appears at 1594 cm^{-1}) bands can expose the amount of disorders in graphenes, especially the sp^3-hybridized defects which normally compared with the sp^2-bonded carbon atoms in a 2D hexagonal lattice. Fig. S2 shows the Raman spectra of as prepared GO and rGO (supporting information). The Raman D and G bands intensity ratio (I_D/I_G ratio) of GO and rGO were calculated as 0.99 and 1.21 respectively. The I_D/I_G ratio of rGO was increased as compared to the GO which indicate the decreasing average size of sp^2 domain concurrently increasing the formation of numerous sp^2 domains in rGO as compared to the GO during the reduction process [32]. This could be due to the elimination of oxygen-containing functional groups during the reduction process. Also, the peaks appeared around 2683 cm^{-1} and 2930 cm^{-1} could be due to the 2D band related to second order of zone-boundary phonons and due to the lattice disorders, respectively [33]. Further, the formation of number of layers can be determined using the shape and peak position of the 2D band appeared in the Raman spectra [34]. The 2D band position of the single-layer rGO sheet was observed at 2678 cm^{-1}, while the 2D band of multilayer shifted to higher frequencies by above 20 cm^{-1} [35]. In our results, the observed 2D band of the rGO sheet was around 2680 cm^{-1} representing the formation of nearly single or few-layer of rGO sheets (supporting information). The Fig. 3a shows Raman spectra recorded from 100 cm^{-1} to 3500 cm^{-1} for bare HTNs and HTNs-rGO composites with different weight percentages of rGO content. The inset in Fig. 3a reveals that the presence of G bands in HTNs-rGO composites which showed that the rGO was successfully incorporated into HTNs matrix. The high intensity peaks appeared at 444 (E_g) and 607 cm^{-1} (A_{1g}) designate the highly crystalline rutile TiO_2 nanorods growth in HTNs-rGO composites. Also the peaks indicated that the growth of crystalline TiO_2 nanorods was not disturbed by the presence of rGO.

The formation of photo-excited charge carriers in HTNs-rGO composite based photoanodes was analyzed by the photoluminescence (PL) spectroscopy. Generally supra-band-gap irradiation of TiO_2 results in emission of photons at specific wavelengths related to either direct band gap, indirect band gap (phonon-assisted), or defect mediated recombination in the TiO_2 crystal. Fig.

3b shows the PL quenching was increased for all HTNs-rGO nanocomposites with respect to increasing rGO content as compared to the bare HTNs; could be due to the lower energy indirect band gap and trap-level-mediated transitions occurred in between HTNs-rGO composites [36]. A reduced electron-hole pair recombination in the HTNs-rGO composites can be attributed to the energy level of rGO lower than the conduction band level of TiO_2, which facilitate the fast transfer of photo-excited electrons from the HTNs to rGO [37]. Further, the PL analysis indicated that the HTNs-rGO composites created a good interfacial contact between HTNs and rGO sheets and reduced the electron-hole pair recombination by the fast transfer of photo-excited electrons from the HTNs to rGO. As a result, the transfer of photo-excited charge carriers enhanced noticeably, which can result in more efficient photovoltaic performance for the HTNs-rGO nanocomposite based DSSCs.

The XPS analysis discloses elements and associated chemical bonds in the top surface (few atomic layers) of the material. Fig. 4a shows wide scan XPS spectra of GO, rGO and HTNs-rGO composite, and in the spectra O 1s, Ti 2p and C 1s peaks are detected at the binding energies 526.8, 461.4 and 283.8 eV, respectively. The C 1s spectrum of the as-prepared GO is deconvoluted into three predominant peaks with binding energies: non-oxygenated rings belong to C-C at 284.73 eV, carbon in C-O (epoxy and hydroxyl) at 285.3 eV and C=O (carbonyl groups) at 287.2 eV [38]. Besides, the C 1s XPS graph of GO (supporting information, Fig. S4) clearly indicates a significant degree of oxidation by showing three components that correspond to carbon atoms bonded with different functional groups. The deconvoluted XPS C 1s spectra of the rGO (Fig. 4b) and HTNs-rGO composite (Fig. 4c) also show the same oxygen functionalities which are assigned for GO. But the peak intensities of these components in the rGO and HTNs-rGO composites are much lower than those in the GO. It shows considerable de-oxygenation happened during the reduction process [39]. The Fig. 4a shows XPS spectra of rutile HTNs-2.0% rGO composite recorded between the binding energy range 700 eV - 200 eV. The Ti 2p, which consists of peaks at 455.7 and 461.4 eV, related to the Ti $2p_{3/2}$ and Ti $2p_{1/2}$ core levels of TiO_2, respectively. The estimated splitting width of 5.7 eV between $Ti2p_{3/2}$ and $Ti2p_{1/2}$ is in good agreement with literature reports [40]. The deconvoluted C 1s XPS spectra of HTNs-2% rGO composite showed binding energy at 283 eV can be accounted to the Ti-O-C bonding interactions. Also from the Fig. 4c it is obvious that the reduction in peak area of C-C bond as

compared to the Ti-O-C bond peak area indicates the growth of TiO_2 nanorods occurred on the rGO sheet surfaces, thus reduces the population of C-C bonds [23].

The Fig. 5 shows HRTEM images of HTNs-2% rGO composite. From the HRTEM images the formation of rGO as folded sheet-like structures after reduction process was confirmed. Fig. 5(b) and (c) shows HRTEM images of HTNs-2% rGO composite. The HRTEM images Fig. 5 (b) and (c) exhibit the TiO_2 nanorods were anchored onto the rGO sheet surface, suggesting that the multi-layered hybrid HTNs-rGO composite architecture was grown on conducting glass substrate up to several micrometers. The Fig. 5d shows an SAED pattern of HTNs-rGO composite, which revealed the as-grown HTNs-rGO, had the combination of highly crystalline rutile TiO_2 nanorod arrays and rGO. Both the higher diffraction intensity of (110) plane of rutile HTNs as compared to the other XRD peaks and its matching d-spacings with SAED pattern d-spacings indicated the [001] direction preferential growth of tetragonal rutile phase nanorod clusters in HTNs. These uniform and dense structures of hybrid HTNs-rGO composites obtained can further support a superior charge transport and collection between the rGO sheets and HTNs in DSSCs. The surface morphologies of the composites, their shapes and growth directions were further analyzed by FESEM. After hydrothermal process the well aligned hierarchical TiO_2 nanorods obtained with and without the presence of rGO are shown Fig. 6a and 6b, respectively. During the hydrothermal process above critical temperature the acid-water mixture generated a uniform solution of precursors of both rGO and titanium (IV) isopropoxide and then induced the formation of an inter-twined or a wrapped HTNs-rGO composite on to the FTO substrate with thicknesses around 14.33 to 15.70 μm, which was confirmed by the FESEM cross-section analysis, as shown in Fig. 6c. The formation of an evenly distributed rGO containing HTNs-rGO composite over the FTO substrate was further confirmed by the energy dispersive spectroscopy (Fig. 6d). The possible growth mechanism for the HTNs-rGO composite on a FTO substrate is schematically illustrated in Scheme 1. In the first step, Ti^{4+} cations from titanium (IV) isopropoxide can favourably intermix with rGO sheets through the electrostatic interactions. In the second step when the temperature increased above 100° C in hydrothermal process, the rapid hydrolysis of titanium (IV) isopropoxide led to the formation of titanium (IV) complex ions and then the dehydration of titanium (IV) complex ions developed nanorod seeds anchored with rGO sheets. Finally, the rGO sheets acted as a base of 2D building block with uniform growth of HTNs through hydrothermal treatment. The TiO_2 nanocrystals seeded on the rGO sheets can play

a key role in the growth of TiO_2 nanorod arrays on to the rGO surface. The uniform and dense TiO_2 nanorod arrays were formed on the rGO sheets because of uniform seed distribution over the rGO sheets. Also, during hydrothermal process the reaction temperature played a significant role in the orientation and development of HTNs, which we already reported in our previous work [11]. When the reaction temperature reached 210 °C, the nanorods grown rGO sheet were deposited on conducting glass substrate as layers. Simultaneously, the TiO_2 molecules formed covalent bonds or intermolecular bonds between rGO and TiO_2 through the rGO functional groups and defect sites, which acted as anchor sites for the crystal growth and resulted in close bonding between the rGO and the HTNs [11, 41].

In order to study the effect of rGO content on the photovoltaic performance of DSSCs fabricated from HTNs loaded with the different wt% of rGO, the J-V measurements were carried out under one sun illumination conditions. The J-V comparison graphs recorded for DSSCs based on various HTNs-rGO composite photoanodes are shown in Fig. 7a and the corresponding power conversion efficiencies of their DSSCs are listed in Table 1. A steady increase in Jsc from 10.04 mA cm^{-2} (HTNs-0.0% rGO) to 12.72 mA cm^{-2} (HTNs-2.0% rGO) was observed for the increase of rGO content up to 2%, as can be seen in the Table 1 and Fig. 7a. However the rGO content above 2% in HTNs-RGO composite DSSC showed a decrease in Jsc value. A sufficient amount of rGO worked as a bridge between the porous structures of HTNs, contributes to the improvement of film roughness and specific surface area, consequently increases the overall dye adsorption of the HTNs-rGO composite photoanodes. Among these nanocomposite photoanodes, the HTNs-2% rGO composite based DSSC device produced a superior open circuit voltage and fill factor as compared to the other HTNs-rGO composites based DSSCs. The improvement in cell performance and the increase of short circuit current density (Jsc) indicated that the solar cell recombination losses were reduced significantly by increasing the wt% of rGO in the HTNs-rGO composites. Also, the rGO had played a key role in facilitating the fast transfer of photo-generated electrons to the FTO substrate in HTNs-rGO composite photoanode which in result increased Jsc. Furthermore, as shown in the Figure 7(c), the IPCE of HTNs-2.0% rGO based DSSC was improved up to 61.4% as compared to the bare HTNs IPCE value of 44.6% at 535 nm (maximum corresponds to the first excitonic absorption of the N719 dye). In general, improvement in IPCE can be evidenced by the enhancement of short circuit current density (Jsc) values of DSSCs. The critical factors considered influencing the IPCE and Jsc values are light

harvesting efficiency, charge separation and collection yields of the electron injected to the FTO substrate of DSSC photoanode [23]. This indicated that the rGO sheets in HTNs-rGO nanocomposites can act as mediators to reduce the charge recombination by forming charge transport channels within the TiO_2 matrix for the easy collection of photogenerated electrons which in result can increase the Jsc of their DSSCs. Thus the HTNs-2.0% rGO based DSSC produced a maximum IPCE due to the better light scattering ability and charge collection yield among HTNs-rGO nanocomposites. Also, these observations were matching to the better PL quenching and charge collection efficiency calculated for the HTNs-2.0% rGO based DSSC from EIS measurements (Table 1). Therefore, the highly conductive rGO was performed as a good charge transfer conduit between TiO_2 nanorods and FTO substrate, which favoured the transfer of more photo-generated electrons from TiO_2 nanorods to FTO without any energy barrier. Also, the high conductivity of rGO can increase the rate of charge transfer process and then diminish the rate of charge recombination, a condition largely desirable for the improvement of PCE in DSSC.

The interfacial charge transfer dynamics at the nanocomposite/electrolyte interface and the enhancement in photocurrent density for HTNs-rGO photoanode was further investigated by the EIS analysis. Fig. 7b shows the EIS spectra of solar cell devices fabricated from the photoanodes of bare HTNs and HTNs-rGO composites with various wt% of rGO. In DSSC EIS Nyquist plot, the large semicircle between 1 to10^3 Hz frequency ranges mainly associated to charge transfer process at the TiO_2/electrolyte interface [42]. The charge transfer generally occurs between electrons in the trap states of TiO_2 conduction band and I_3^- ions in the electrolyte medium. To analyze the EIS Nyquist plot we constructed an equivalent circuit to characterize the series resistance (R_s) and charge transfer resistance (R_{ct}) at the TiO_2-electrolyte interface of the DSSCs. As shown in Fig. 7b, compared to the bare HTNs photoanode R_{ct} value was drastically decreased for the HTNs-2.0% rGO composites. Moreover, the charge collection efficiency (η_{cc}) values for the nanocomposite photoanodes were calculated from the measured impedance data using the equation [42] $\eta_{coll}=1/[1+(R_{tr}/R_{ct})]$, R_{tr} is the charge transport resistance of electrons through the HTNs and rGO in the nanocomposite film which can be estimated from the Nyquist plots of the EIS obtained under illumination at the open circuit voltage. The higher η_{cc} values obtained for the HTNs-rGO composite photoanodes as compared to that of bare HTNs photoanode revealed the better charge transfer and collection due to the presence of rGO conduit. Furthermore the

Bode phase plots of DSSCs of bare HTNs and HTNs-rGO composites obtained from the impedance spectroscopy are given in Fig. S5 in supporting information and from Bode plots the calculated electron (charge carrier) lifetime values correspond to the different nanocomposite photoanodes are listed in Table 1. The mean electron lifetime (τ_e) calculated using the equation $\tau_e=1/(2\pi f_{max})$ for DSSCs of bare HTNs and HTNs-rGO composites showed a longer lifetime and slower recombination process for HTNs-rGO composite based DSSCs. These results clearly indicate that the charge collection efficiency and power conversion efficiency in HTNs-rGO composite based DSSCs were improved due to the presence of rGO. Moreover, the EIS analysis revealed that the incorporation of rGO sheets in the nanocomposite facilitated a superior charge separation and transport in the nanocomposite photoanodes, which resulted in the overall photovoltaic performance enhancement of hierarchical TiO_2 nanorods based DSSCs.

4. Conclusions

In summary, we demonstrated the fabrication of various HTNs-rGO composites based photoanodes for the use in DSSCs. The in-situ growth of TiO_2 and rGO uniformly on conducting glass substrate were confirmed by the spectroscopic and microscopic characterizations. Particularly the presence of rGO in HTNs matrix was confirmed by UV-visible diffused reflectance, Raman and HRTEM analyses. Weight ratio of rGO with respect to the HTNs was varied to determine the effect of rGO content on the photovoltaic and EIS parameters of HTNs-rGO nanocomposite based DSSCs. A high PCE of 4.54% was achieved in DSSC device fabricated using the HTNs with 2.0 wt% rGO incorporated photoanode. The PCE was improved 47.8% for the DSSC prepared with HTNs-2.0% rGO photoanode as compared to the bare HTNs DSSC; it was mainly attributed to the increase of J_{sc} and FF due to the enhanced charge separation and transport, a conclusion arrived from the EIS, IPCE and PL studies. But in the experiments, a higher rGO content (2.8 wt%) in the nanocomposite photoanode showed a decreased J_{sc}, possibly due to the higher rGO content reduced photon harvesting of dye molecules and increased the participation of rGO in the recombination kinetics. Finally, these results indicated that the HTNs-rGO based photoanode with optimal loading (2 wt%) of rGO can enhance DSSC PCE significantly due to the superior charge transfer conduit formation by the rGO in HTNs matrix.

Acknowledgements

Financial support from DRDO and DST CERI for this work is gratefully acknowledged. M. R. S thanks Dr. T. G. Manivasagam and Dr. M. Rangarajan for their support in EIS measurements. D. K. thanks SAIF, IITM for providing SEM and XRD facilities and Amrita Nanoscience Center, Kochi for the support in HRTEM analysis.

References

[1] J. Burschka, N. Pellet, S.J. Moon, R. Humphry-Baker, P. Gao, M.K. Nazeeruddin, M. Gratzel, Sequential deposition as a route to high-performance perovskite-sensitized solar cells, Nature, 499 (2013) 316-319.

[2] A. Pandikumar, S.-P. Lim, S. Jayabal, N.M. Huang, H.N. Lim, R. Ramaraj, Titania@gold plasmonic nanoarchitectures: An ideal photoanode for dye-sensitized solar cells, Renewable and Sustainable Energy Reviews 60 (2016) 408–420.

[3] A. Yella, H.W. Lee, H.N. Tsao, C. Yi, A.K. Chandiran, M.K. Nazeeruddin, E.W.G. Diau, C.Y. Yeh, S.M. Zakeeruddin, M. Grätzel, Porphyrin-sensitized solar cells with cobalt (II/III)-based redox electrolyte exceed 12 percent efficiency, Science 80 (2011) 629–634.

[4] S. Mathew, A. Yella, P. Gao, R. Humphry-Baker, F.E. CurchodBasile, N. Ashari Astani, I. Tavernelli, U. Rothlisberger, M.K. Nazeeruddin, M. Grätzel, Dye-sensitized solar cells with 13% efficiency achieved through the molecular engineering of porphyrin sensitizers, Nature Chemistry, 6 (2014) 242-247.

[5] K. Rokesh, A. Pandikumar, K. Jothivenkatachalam, Dye sensitized solar cells: A summary, Materials Science Forum, 771 (2014) 1-24.

[6] N. Tetreault, M. Gratzel, Novel nanostructures for next generation dye-sensitized solar cells, Energy & Environmental Science, 5 (2012) 8506-8516.

[7] X. Wang, Z. Li, J. Shi, Y. Yu, One-dimensional titanium dioxide nanomaterials: nanowires, nanorods, and nanobelts, Chemical Reviews, 114 (2014) 9346-9384.

[8] A. Kumar, A.R. Madaria, C. Zhou, Growth of aligned single-crystalline rutile TiO_2 nanowires on arbitrary substrates and their application in dye-sensitized solar cells, The Journal of Physical Chemistry C, 114 (2010) 7787-7792.

[9] M. Law, L.E. Greene, J.C. Johnson, R. Saykally, P. Yang, Nanowire dye-sensitized solar cells, Nature Materials, 4 (2005) 455-459.

[10] Y. Gao, M. Nagai, T.C. Chang, J.J. Shyue, Solution-derived ZnO nanowire array film as photoelectrode in dye-sensitized solar cells, Crystal Growth Design, 7 (2007) 2467–2471.

[11] M.R. Subramaniam, S. Devanathan, D. Kumaresan, Synthesis of micrometer-sized hierarchical rutile TiO_2 flowers and their application in dye sensitized solar cells, RSC Advances, 4 (2014) 36791-36799.

[12] H. Wang, S.L. Leonard, Y.H. Hu, Promoting Effect of graphene on dye-sensitized solar cells, Industrial & Engineering Chemistry Research, 51 (2012) 10613-10620.

[13] K.S. Novoselov, A.K. Geim, S.V. Morozov, D. Jiang, Y. Zhang, S.V. Dubonos, I.V. Grigorieva, A.A. Firsov, Electric field effect in atomically thin carbon films, Science, 306 (2004) 666-669.

[14] C. Lee, X. Wei, J.W. Kysar, J. Hone, Measurement of the elastic properties and intrinsic strength of monolayer graphene, Science, 321 (2008) 385-388.

[15] E. Yoo, J. Kim, E. Hosono, H.S. Zhou, T. Kudo, I. Honma, Large reversible Li storage of graphene nanosheet families for use in rechargeable lithium ion batteries, Nano Letters, 8 (2008) 2277-2282.

[16] S.P. Lim, A. Pandikumar, Y.S. Lim, N.M. Huang, H.N. Lim In-situ electrochemically deposited polypyrrole nanoparticles incorporated reduced graphene oxide as an efficient counter electrode for platinum-free dye-sensitized solar cells, Scientific Reports 4 (2014) 5305.

[17] F.A. Jumeri, H.N. Lim, Z. Zainal, N.M. Huang, A. Pandikumar, S.P. Lim Dual functional reduced graphene oxide as photoanode and counter electrode in dye-sensitized solar cells and its exceptional efficiency enhancement, Journal of Power Sources 293 (2015) 712-720.

[18] J. Shen, B. Yan, M. Shi, H. Ma, N. Li, M. Ye, One step hydrothermal synthesis of TiO_2-reduced graphene oxide sheets, Journal of Materials Chemistry, 21 (2011) 3415-3421.

[19] M. Khannam, S. Sharma, S. Dolui, S.K. Dolui, Graphene oxide incorporated TiO_2 photoanode for high efficiency quasi solid state dye sensitized solar cells based on poly-vinyl alcohol gel electrolyte, RSC Advances, (2016) 55406-55414.

[20] S.B. Kim, J.Y. Park, C.S. Kim, K. Okuyama, S.E. Lee, H.D. Jang, T.O. Kim, Effects of graphene in dye-sensitized solar cells based on nitrogen-dopedTiO_2 composite, Journal of Physical Chemistry C 119 (2015) 16552–16559.

[21] S. Sun, L. Gao, Y. Liu, Enhanced dye-sensitized solar cell using graphene-TiO_2 photoanode prepared by heterogeneous coagulation, Applied Physics Letters, 96 (2010) 083113.

[22] S.P. Lim, A. Pandikumar, N.M. Huang, H.N. Lim, Reduced graphene oxide–titania nanocomposite-modified photoanode for efficient dye-sensitized solar cells, International Journal of Energy Research, 39 (2015) 812-824.

[23] E. Nouri, M.R. Mohammadi, P. Lianos, Impact of preparation method of TiO2-RGO nanocomposite photoanodes on the performance of dye-sensitized solar cells, Electrochimica Acta 219 (2016) 38–48.

[24] J. Liu, H. Bai, Y. Wang, Z. Liu, X. Zhang, D.D. Sun, Self-assembling TiO_2 nanorods on large graphene oxide sheets at a two-phase interface and their anti-recombination in photocatalytic applications. Advanced Functional Materials 20 (2010) 4175–4181.

[25] D. Li, M.B. Muller, S. Gilje, R.B. Kaner, G.G. Wallace, Processable aqueous dispersions of graphene nanosheets, Nature Nanotechnology, 3 (2008) 101-105.

[26] Y. Liu, Hydrothermal synthesis of TiO_2-rGO composites and their improved photocatalytic activity in visible light, RSC Advances, 4 (2014) 36040-36045.

[27] W.S. Wang, D.H. Wang, W.G. Qu, L.Q. Lu, A.W. Xu, Large ultrathin anatase TiO_2 nanosheets with exposed {001} facets on graphene for enhanced visible light photocatalytic activity, The Journal of Physical Chemistry C, 116 (2012) 19893-19901.

[28] Y. Kusumawati, M.A. Martoprawiro, T. Pauporté, Effects of graphene in graphene/TiO_2 composite films applied to solar cell photoelectrode, The Journal of Physical Chemistry C, 118 (2014) 9974-9981.

[29] X.Y. Zhang, H.P. Li, X.L. Cui, Y. Lin, Graphene/TiO_2 nanocomposites: synthesis, characterization and application in hydrogen evolution from water photocatalytic splitting, Journal of Materials Chemistry, 20 (2010) 2801-2806.

[30] Z. Xiang, X. Zhou, G. Wan, G. Zhang, D. Cao, Improving energy conversion efficiency of dye-sensitized solar Cells by modifying TiO_2 photoanodes with nitrogen-reduced graphene oxide, ACS Sustainable Chemistry & Engineering, 2 (2014) 1234-1240.

[31] D. Wang, D. Choi, J. Li, Z. Yang, Z. Nie, R. Kou, D. Hu, C. Wang, L.V. Saraf, J. Zhang, I.A. Aksay, J. Liu, Self-assembled TiO_2-graphene hybrid nanostructures for enhanced Li-ion insertion, ACS Nano, 3 (2009) 907-914.

[32] S. Stankovich, D.A. Dikin, R.D. Piner, K.A. Kohlhaas, A. Kleinhammes, Y. Jia, Y. Wu, S.T. Nguyen, R.S. Ruoff, Synthesis of graphene-based nanosheets via chemical reduction of exfoliated graphite oxide, Carbon, 45 (2007) 1558-1565.

[33] V.C. Tung, M.J. Allen, Y. Yang, R.B. Kaner, High-throughput solution processing of large-scale graphene, Nature Nanotechnology, 4 (2009) 25-29.

[34] K.N. Kudin, B. Ozbas, H.C. Schniepp, R.K. Prud'homme, I.A. Aksay, R. Car, Raman spectra of graphite oxide and functionalized graphene sheets, Nano Letters, 8 (2008) 36-41.

[35] D. Graf, F. Molitor, K. Ensslin, C. Stampfer, A. Jungen, C. Hierold, L. Wirtz, Spatially resolved raman spectroscopy of single and few-layer graphene, Nano Letters, 7 (2007) 238-242.

[36] N.D. Abazović, M.I. Čomor, M.D. Dramićanin, D.J. Jovanović, S.P. Ahrenkiel, J.M. Nedeljković, Photoluminescence of anatase and rutile TiO_2 particles, The Journal of Physical Chemistry B, 110 (2006) 25366-25370.

[37] J. Liu, H. Bai, Y. Wang, Z. Liu, X. Zhang, D.D. Sun, Self-assembling TiO_2 nanorods on large graphene oxide sheets at a two-phase interface and their anti-recombination in photocatalytic applications, Advanced Functional Materials, 20 (2010) 4175-4181.

[38] S. Ghasemi, A. Esfandiar, S. Rahman Setayesh, A. Habibi Yangjeh, A. Iraji zad, M.R. Gholami, Synthesis and characterization of TiO_2-graphene nanocomposites modified with noble metals as a photocatalyst for degradation of pollutants, Applied Catalysis A: General, 462-463 (2013) 82-90.

[39] S. Stankovich, R.D. Piner, X. Chen, N. Wu, S.T. Nguyen, R.S. Ruoff, Stable aqueous dispersions of graphitic nanoplatelets via the reduction of exfoliated graphite oxide in the presence of poly(sodium 4-styrenesulfonate), Journal of Materials Chemistry, 16 (2006) 155-158.

[40] A. Ramadoss, G.S. Kim, S.J. Kim, Fabrication of reduced graphene oxide/TiO_2 nanorod/reduced graphene oxide hybrid nanostructures as electrode materials for supercapacitor applications, CrystEngComm, 15 (2013) 10222-10229.

[41] R. Zou, Z. Zhang, L. Yu, Q. Tian, Z. Chen, J. Hu, A general approach for the growth of metal oxide nanorod arrays on graphene sheets and their applications, Chemistry-A European Journal, 17 (2011) 13912-13917.

[42] M.R. Subramaniam, D. Kumaresan, CdSe Quantum Dots and N719-Dye Decorated Hierarchical TiO_2 Nanorods for the Construction of Efficient Co-Sensitized Solar Cells, ChemPhysChem, 16 (2015) 2543-2548.

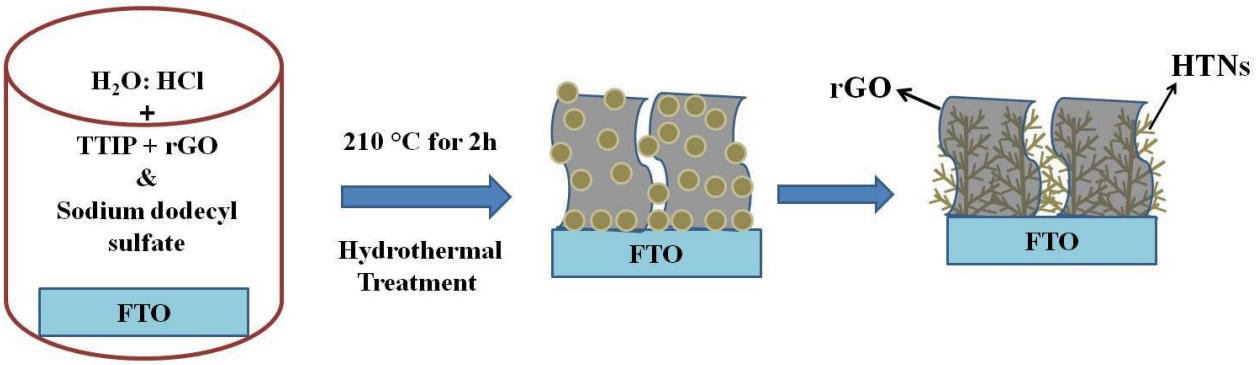

Scheme 1: Schematic illustration of nucleation and growth of rGO wrapped hierarchical TiO_2 on FTO substrate by in situ hydrothermal process

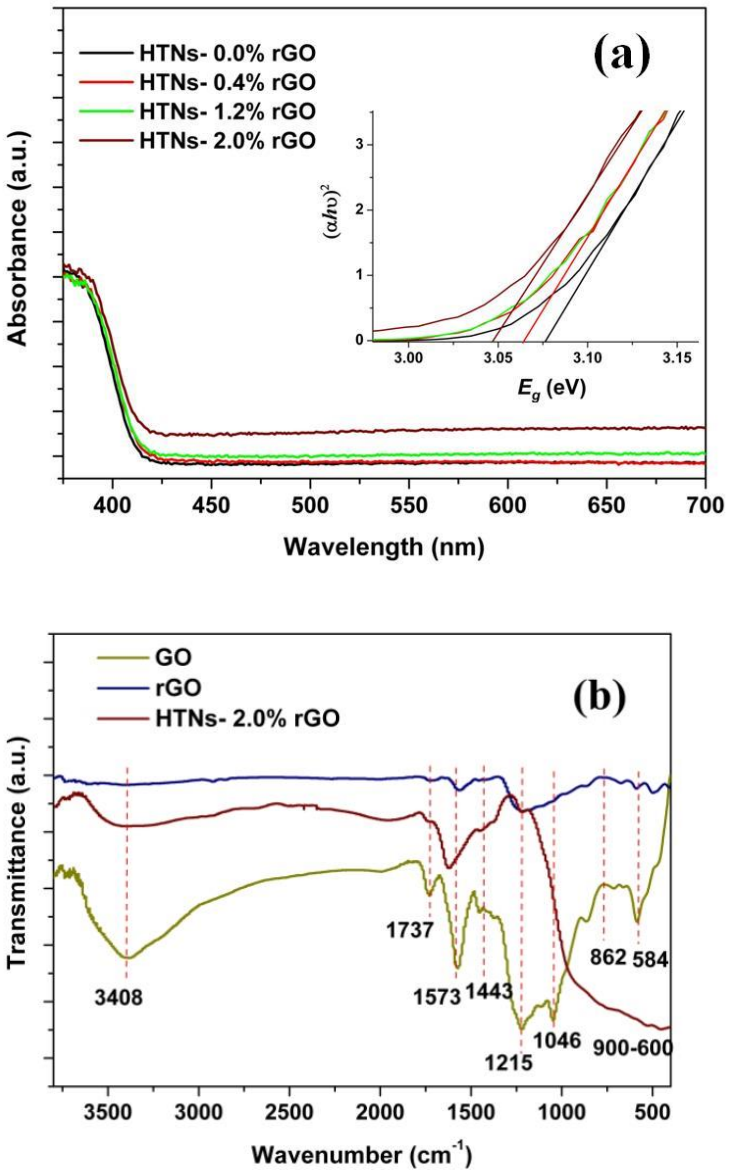

Fig. 1 (a) UV-visible absorption spectra of HTNs and HTNs-rGO composite based photoanode films (Inset: Tauc plot) (b) FTIR spectra of GO, rGO and HTNs-2.0% rGO.

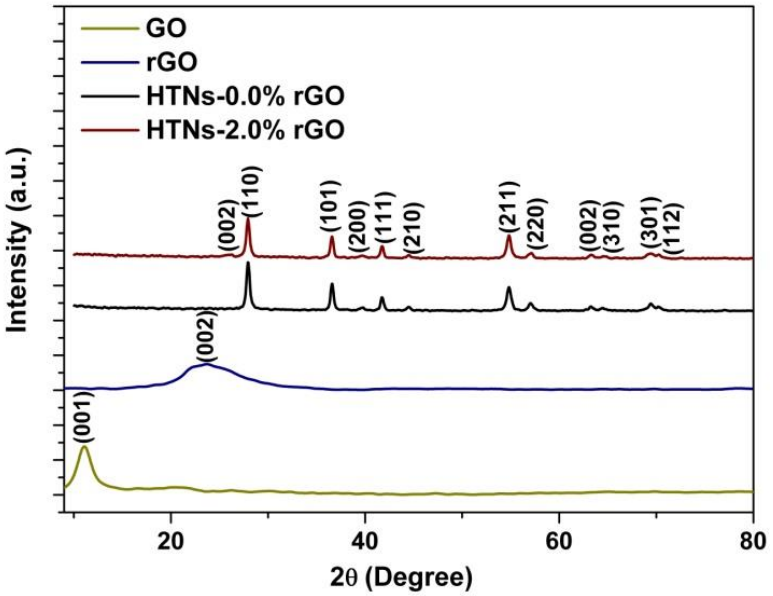

Fig. 2 XRD pattern of GO, rGO, HTNs and HTNs-2.0% rGO composite

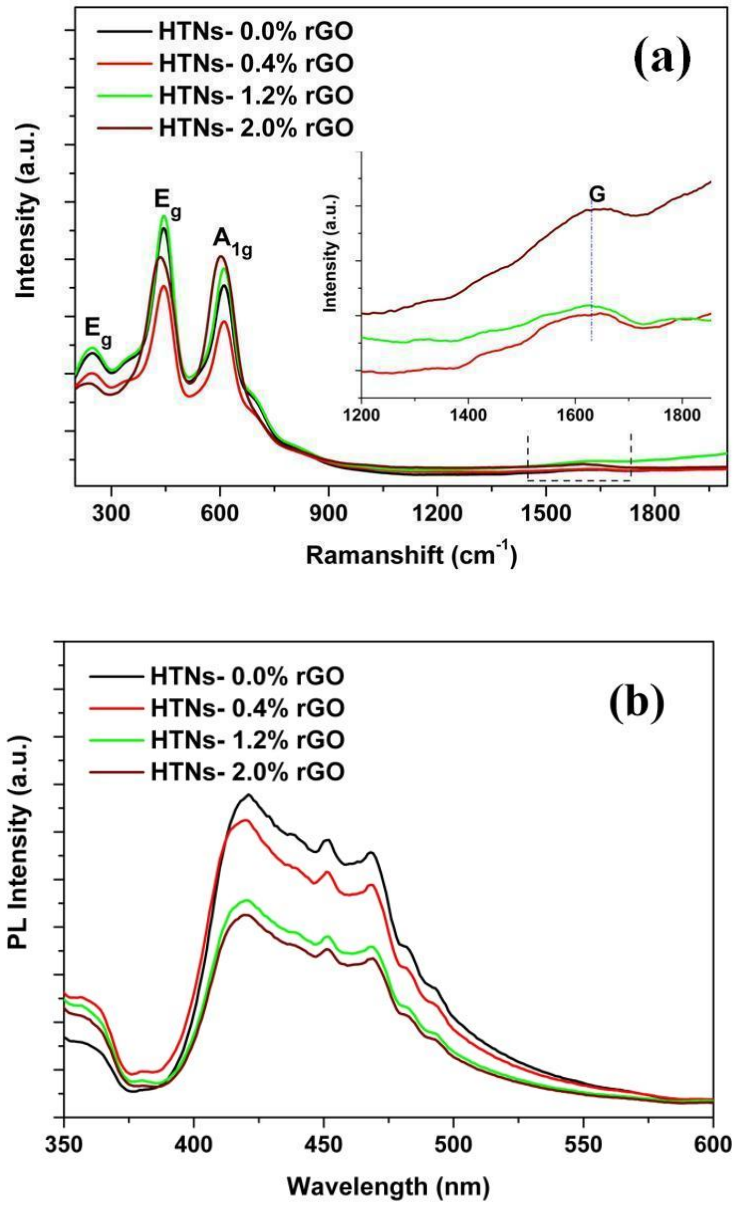

Fig. 3 (a) Raman spectra of HTNs-rGO composites in different rGO weight ratios [Inset: G band of rGO] (b) PL spectra of HTNs and HTNs-rGO composite based photoanodes

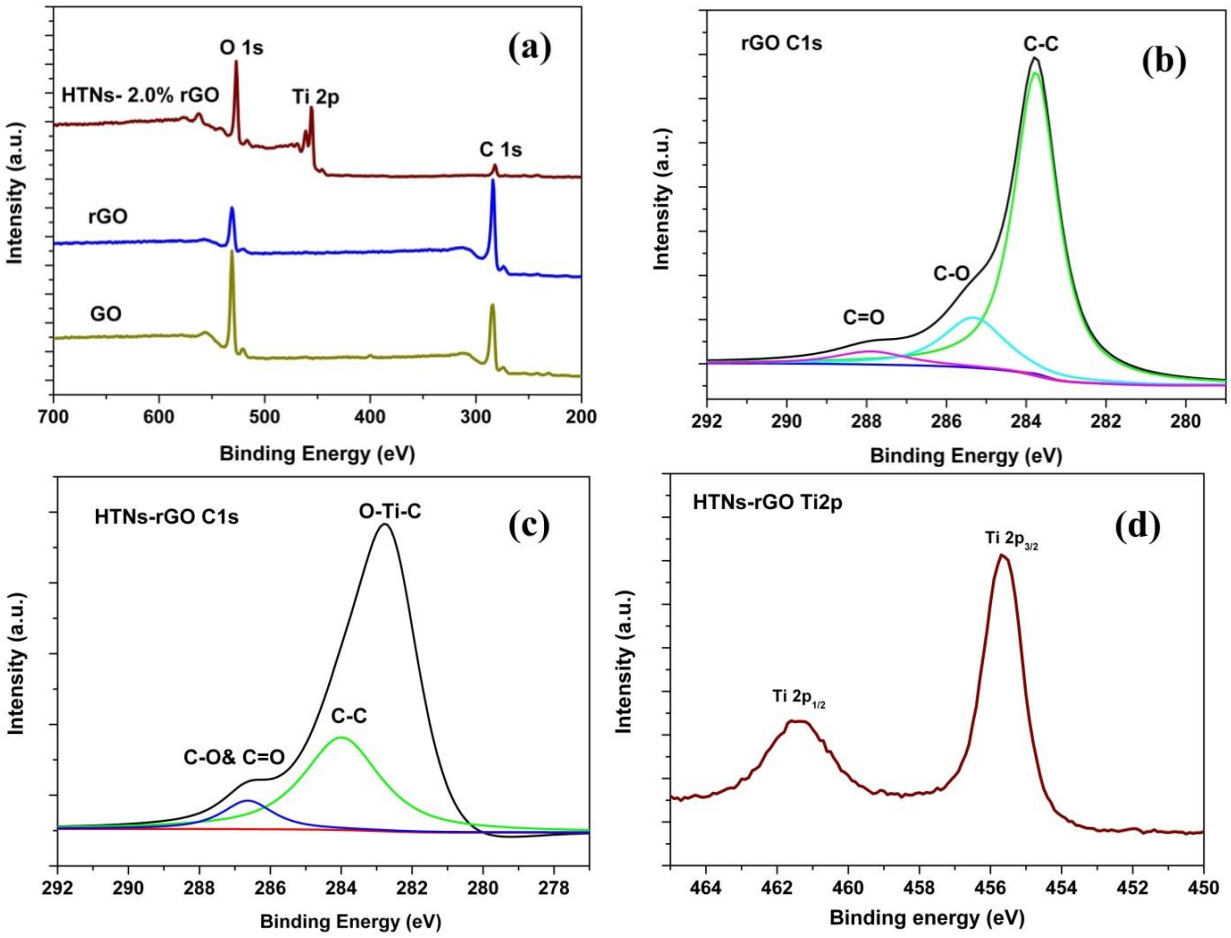

Fig. 4 (a) XPS spectra of wide survey scan of GO, rGO and HTNs-2.0 % rGO, (b) and (c) Deconvoluted C 1s XPS spectra of rGO and HTNs-2% rGO composite, respectively (d) Deconvoluted Ti 2p XPS spectrum of HTNs-2.0% rGO composite

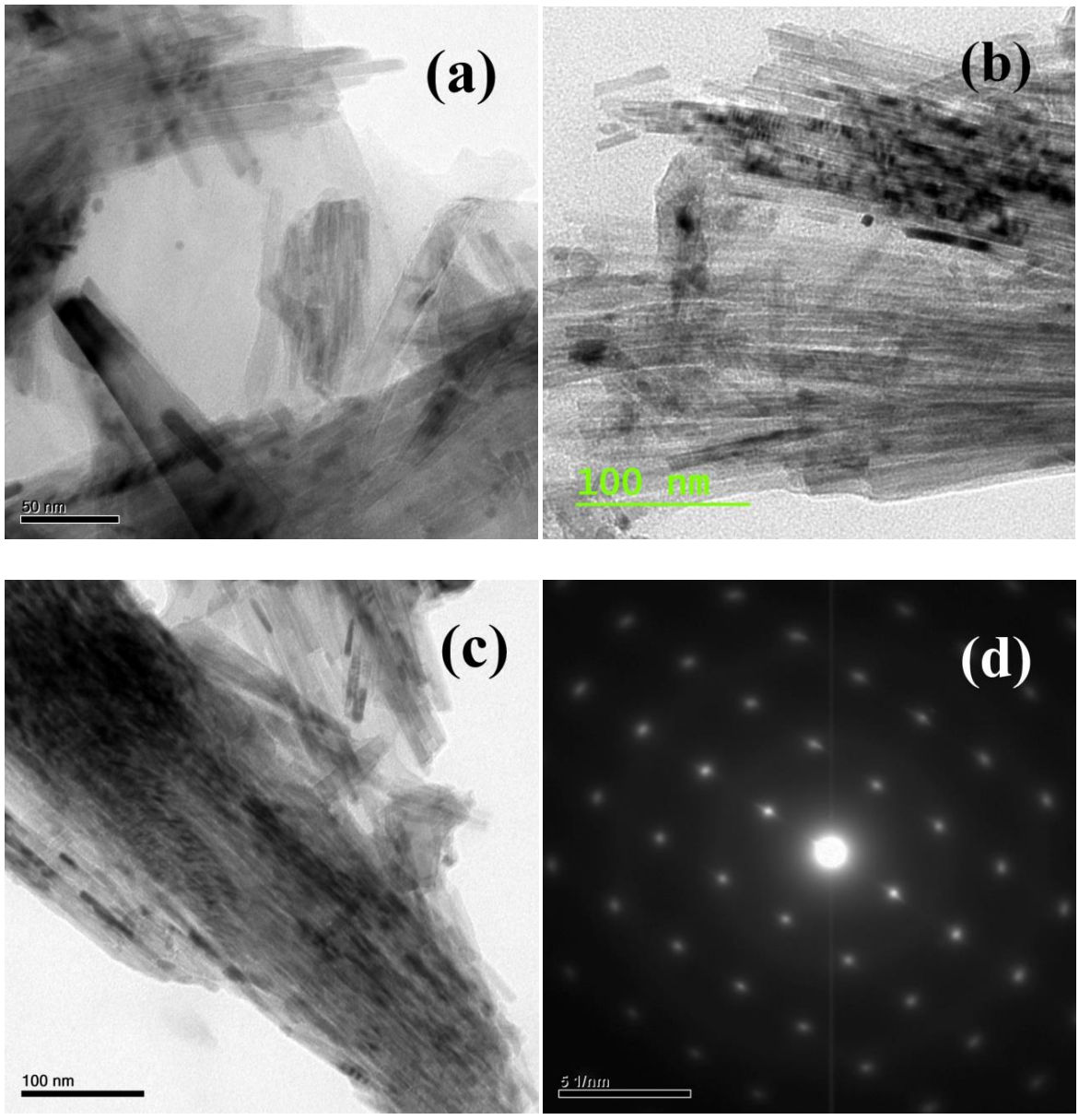

Fig. 5 HR-TEM images of (a), (b) and (c) HTNs-2.0% rGO, and (d) SAED pattern of HTNs-2.0% rGO composite

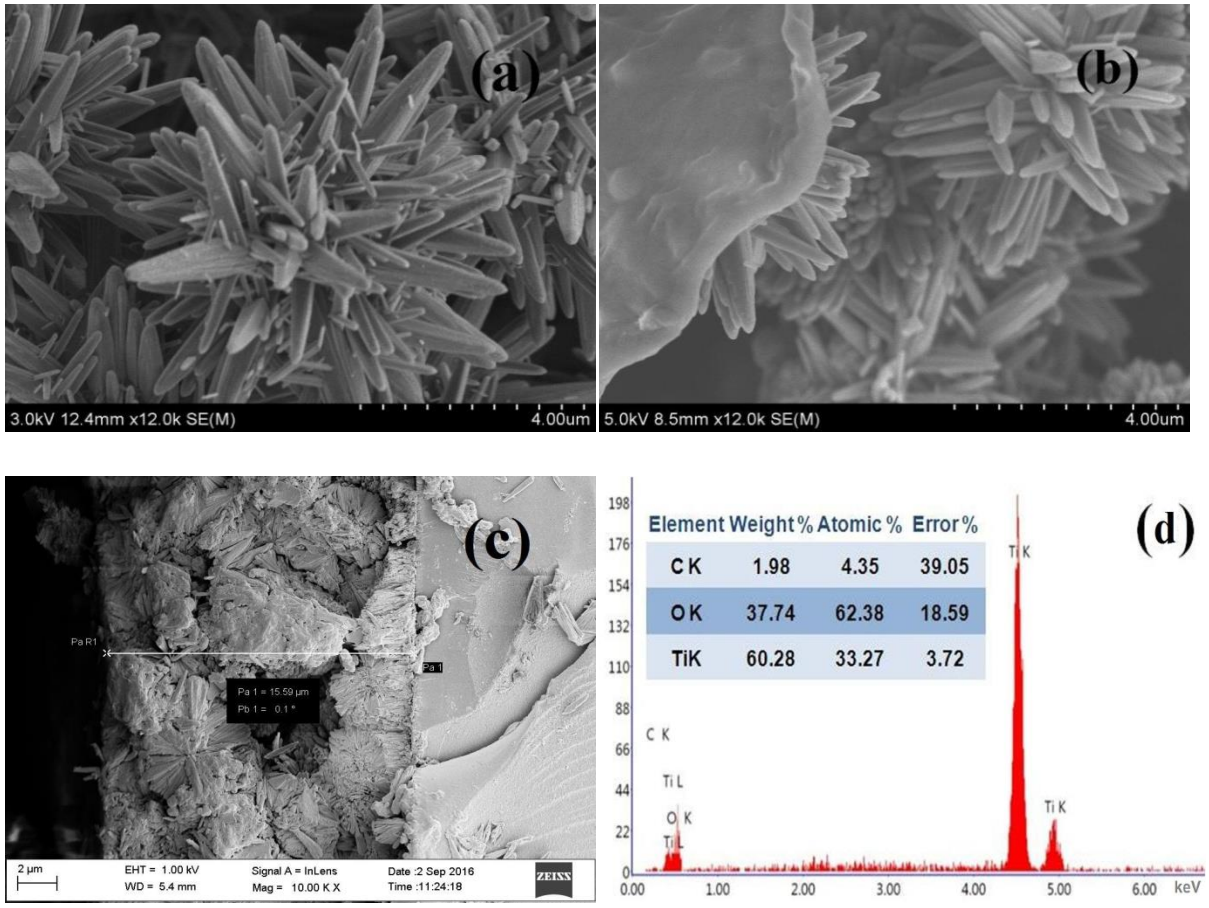

Fig. 6 FESEM images of (a) HTNs (b) HTNs- 2.0% rGO composite, (c) Cross section view of HTNs- 2.0% rGO composite on FTO and (d) EDS chemical composition of HTNs-2.0% rGO composite

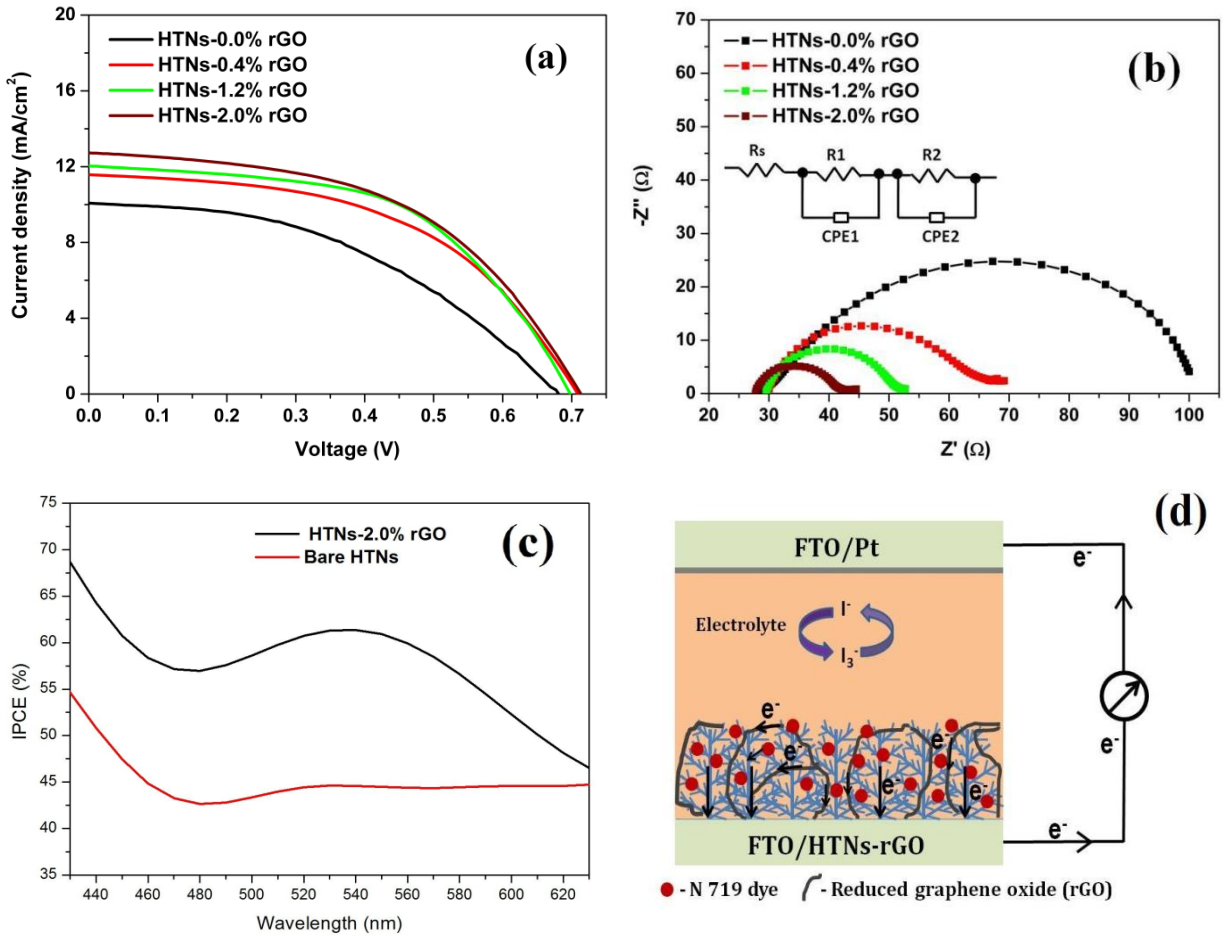

Fig. 7 (a) Comparative J-V curves of HTNs and HTNs-rGO nanocomposites based DSSCs (b) Nyquist plots of the DSSCs made of HTNs and HTNs-rGO composites recorded in one sun illumination conditions and (c) IPCE spectra of HTNs-2% rGO and

bare HTNs based DSSCs (d) Schematic illustration of charge transport processes involved in the HTNs-rGO nanocomposite photoanode based DSSCs.

Table 1. Under illumination EIS parameters and power conversion efficiencies of different HTNs-rGO composite based DSSCs.

Sample	**R_s (ohm cm^2)**	**R_{ct} (ohm cm^2)**	**R_{tr} (ohm cm^2)**	**Charge Collection Efficiency (%)**	**Electron lifetime (μs)**	**Power conversion efficiency (%)**
HTNs-0.0 % rGO	28.13	67.41	2.63	96.24	31	3.07
HTNs-0.4 % rGO	29.71	36.67	0.90	97.60	46	4.03
HTNs-1.2 % rGO	29.56	22.67	0.28	98.77	47	4.35
HTNs-2.0 % rGO	27.79	14.56	0.40	97.32	73	4.54

[#]All solar cells showed near matching open circuit voltage of 0.68-0.70 V with fill factor (FF) in the range of 0.48-0.52.